Applied Thermal Engineering 280 (2025) 128229

Contents lists available at ScienceDirect

Applied Thermal Engineering

journal homepage: www.elsevier.com/locate/apthermeng

Research Paper

Energy-saving retrofit and thermal economy optimization of peak-shaving for coal-fired power plants utilizing molten salt thermal storage

Qilong Xu [a], Shuai Wang [a,b], Kun Luo [a,b,*], Jianren Fan [a,b]

[a] State Key Laboratory of Clean Energy Utilization, Zhejiang University, Hangzhou 310027, China
[b] Shanghai Institute for Advanced Study of Zhejiang University, Shanghai 200120, China

ARTICLE INFO

Keywords:
Peak shaving
Molten salt thermal energy storage
Energy-saving retrofit
Process simulation
Sensitivity analysis
Thermal economy optimization

ABSTRACT

Flexibility retrofitting of coal-fired power plants (CFPPs) consumes a high proportion of unstable energy power, leading to the increased energy consumption of the retrofitted system. Therefore, it is of great significance to optimize the energy saving performance of CFPPs after flexibility retrofitting. In this study, the energy-saving design of a molten salt thermal energy storage (MSTES) peak-shaving system for a supercritical CFPP is optimized. First, an integrated peak-shaving model of a 600 MW supercritical CFPP with MSTES is developed. Then, a synergistic energy-saving strategy incorporating the No. 0 high-pressure heater (HPH) and the front steam cooler (FSC) is introduced into the coupled model to reduce the energy consumption of the peak-shaving system, thereby overcoming the conventional trade-off between peak-shaving depth and coal consumption. The arrangement of these two energy-saving methods is further optimized. In addition, the thermoeconomic mechanism at the 6 MPa critical pressure point is revealed, characterized by a dynamic balance between turbine exhaust steam enthalpy drop and heating benefits, which determines the optimal exhaust steam pressure for the heat storage/release process. Finally, the performance of the improved peak-shaving model is evaluated. The results indicate reducing the superheat temperature of the No. 3 exhaust steam via the FSC from 210–240 °C increases boiler efficiency by 0.60 %. After accounting for auxiliary power consumption, the net peak shaving depth reaches 9.51 % under 40 % turbine heat acceptance conditions, while the net coal consumption rate decreases by 1.16–1.85 g/kWh. These findings provide valuable guidance for enhancing the power generation efficiency of peak-shaving systems in retrofitted CFPPs.

1. Introduction

In the past decade, China's renewable energy, represented by wind and solar energy, has developed rapidly, with the newly installed scale of wind and solar power reaching 205 million kilowatts in 2023, accounting for 62.1 % of the country's newly installed capacity [1–3]. However, the intermittency and uncertainty characteristics of high-penetration renewable energy generation have brought serious challenges to the stable operation of the power grid, resulting in increasingly prominent power system volatility [4]. Currently, thermal power generation still occupies a dominant position by virtue of its stability and reliability, in which coal-fired power generation is still the main mode of power generation, while regulated power sources (including fuel oil, natural gas and pumped storage, etc.) account for less than 6 % [5,6]. For this reason, it is crucial to implement flexibility modification of coal-fired power plants (CFPPs) to adapt to the demand for new energy grid connections and build a new type of power system [7,8]. In the new power system with new energy as the main body, the role of CFPPs has been gradually changed from the baseload power supply to the main power source to provide reliable capacity, power and flexibility to regulate the support power source, which plays an important role in the peak of the power system [9,10].

Since CFPPs were not initially designed for high-frequency, deep load regulation, there are deficiencies in spatiotemporal matching of energy and mass flows [11]. As a result, the response speed and depth of the peak-shaving process of traditional CFPPs are obviously insufficient when responding to the grid regulation demand of frequent load changes [12]. Currently, significant progress has been made in the retrofit technology of CFPPs, which mainly includes boiler-side combustion system retrofit and turbine system retrofit [13–15]. However, these modifications are complex and difficult to realize in actual power plants. Therefore, in order to stabilize power supply, there is an urgent

* Corresponding author at: State Key Laboratory of Clean Energy Utilization, Zhejiang University, Hangzhou 310027, China.
E-mail address: zjulk@zju.edu.cn (K. Luo).

https://doi.org/10.1016/j.applthermaleng.2025.128229
Received 17 June 2025; Received in revised form 12 August 2025; Accepted 3 September 2025
Available online 6 September 2025

need to couple CFPPs with energy storage systems that have flexible peak shifting capabilities [16,17]. Among them, the peak-shaving method that combines CFPPs with molten salt thermal energy storage (MSTES) can not only significantly improve the peak-shaving capacity, but also ensure that the economy of thermal power units will not be significantly reduced [18–20]. Peak-shaving technology of MSTES utilizes the excellent thermal storage performance of molten salt to store the excess thermal energy generated during the operation of the system and release it in time when the load demand of the grid peaks, thus realizing deep peak-shaving. This peak-shaving method not only helps to extend the service life of CFPPs, but also significantly improves the peak-shaving efficiency and reduces the dependence on traditional peak-shaving technology [21,22]. Therefore, MSTES has become a key retrofitting approach to enhance the flexibility of CFPPs, providing a strong support for the stable operation of the new power system [23,24].

The research on the multi-scenario application of MSTES has made a series of breakthroughs in recent years. In the field of solar photovoltaic, Zhang et al [25] addressed the issue of energy consumption for the startup of a molten salt-worked photovoltaic power plant, revealing that the energy loss of the power plant mainly originates from the collector optical loss (45.80 %), the turbine cold source loss (23.11 %), and the receiver heat loss (17.91 %) through the exergy analysis, and put forward a low-load regenerative heater scheme, which provides theoretical support for the optimization of the startup of the power plant; Hood et al [26] investigated the thermal fatigue of a molten salt-steam heat exchanger in a concentrated solar power (CSP) tower power plant, and the results showed that the expected lifetimes of the evaporator and superheater under typical fast peak-shaving operation were 10 and 25 years, respectively, which were significantly lower than the design lifetime of 30 years. This study provides a scientific basis for optimizing power station scheduling and extending equipment life; Oriented to the peak demand of CFPPs, Xu et al [27] compared five heat storage schemes and found that the purely electric heat production (P2H) scheme can achieve zero power output, with an equivalent round-trip efficiency of 36.23 %, but limited by the electric heating exergy loss, exergy efficiency is only 36.51 %, whereas the efficiency of the coupled system of heat storage exergy efficiency is improved to 39.58 %; Jiang et al [19] developed a new type of flue gas-molten salt heat exchanger (FMHE), which was verified through dynamic modeling to maintain the quality of heat storage in 100 %-80 % load regulation, and to solve the thermal hysteresis effect and temperature control problems. Zhang et al [28] proposed a synergistic peak-shaving strategy of steam extraction coupled with molten salt storage, and found that the main steam and feedwater reheat scheme had the optimal heat storage efficiency, with a peak-shaving depth of 12.83 %Pe, with a retrofit cost of US$19.948 million. Wang et al [29] further explored the effect of molten salt heat storage temperature on the flexibility of CFPPs, constructed four integration modes, and found that reducting the heat storage temperature from 480 °C to 309 °C improves the recharge efficiency by 17 %, and extends the discharging time by 23 %.

From the above studies, it can be seen that with the surge in demand for power system regulation due to the high proportion of renewable energy connected to the grid, MSTES has become an important technology path for the flexibility retrofit of CFPPs. However, there are still key gaps in existing research. Due to high steam parameters, supercritical units have 40–60 % higher steam extraction superheat than subcritical power plants [30], and traditional molten salt retrofitting solutions exacerbate heat loss under these conditions, causing the industry to face the dilemma of more coal consumption for peak shaving [31].Most of the existing research focuses on the thermal storage capacity and the enhancement of the peak-shaving depth, lacks the systematic analysis of the thermal economy of the peak-shaving system and energy-saving optimization [32,33].

Therefore, it is difficult to realize the synergistic optimization of peak-shaving capacity and energy consumption control by simply relying on the expansion of the thermal storage system, and the trade-off between peak-shaving capacity and energy efficiency must be solved through the energy-saving modification of the key equipment of the thermal system and the refinement of the design of the operation strategy [34]. To address this contradiction, this study proposes an energy-saving framework that integrates a front steam cooler with the No. 0 high-pressure heater, with the following objectives: 1) the optimization design of coal consumption of 600 MW supercritical CFPP peak-shaving system with MSTES; 2) to establish design criteria for deep peak load regulation based on thermal economic optimization, and provide theoretical basis and technical support for its efficient peak-shaving and thermal economy optimization.

In this research, firstly, the integrated model of 600 MW supercritical CFPP with MSTES is constructed. Second, in order to optimize the thermal economy of the peak-shaving system, this study innovatively proposes a synergistic energy-saving method for molten salt thermal energy storage peak shaving systems (the No. 0 high-pressure heater (HPH) and front steam cooler (FSC) technologies) into the coupled model to reduce the energy consumption of the peak-shaving system [35], overcoming the bottleneck between peak shaving depth and coal consumption in traditional schemes. Specifically, the No. 0 HPH is responsible for recovering part of the exhaust heat and storing it in the molten salt during low load operation, while the FSC serves as an auxiliary device for rapid heat release during high load. This design not only improves the heat conversion efficiency of the MSTES, but also significantly reduces the response time of the system at peak loads, thus enhancing the practical application of the peak-shaving model. The optimized peak-shaving model helps the CFPP to achieve more efficient and stable operation in response to the peak and valley fluctuations of the power grid [36].

Finally, for the energy-saving retrofitted peak-shaving scheme, the impact of different key parameters on the amount of coal consumption of the unit is analyzed in terms of sensitivity and the optimal parameters are obtained, and the peak-shaving performance of the retrofitted peak-shaving model is evaluated through simulation calculations. For a 600 MW supercritical unit, this study first reveals the thermo-economic mechanism at the 6 MPa critical pressure point (dynamic balance between steam extraction enthalpy drop and heating benefits), establishing the optimal steam extraction pressure for the heat storage/release process. This scheme provides low-cost regulation capability for grids with high proportions of renewable energy, driving the transformation of coal-fired plant from a primary power source to a regulatory support role.

The reminder of this paper is as follows: Section 2 describes the construction of the coupled peak-shaving model of CFPP and the design of the energy-saving method; Section 3 explores the influence of the steam extraction port position (SEPP) and the change of the feedwater temperature of the heat storage and release process on the thermal economy and the analysis of the peak-shaving performance (thermodynamic performance and economic performance) after the energy-saving modification. The conclusion section summarizes the role of this optimization scheme in enhancing the flexibility and economy of CFPPs, and provides new ideas for future peak-shaving applications in coal-fired power plants.

2. Energy-saving retrofit schemes design of coupled peak-shaving model

2.1. Modelling and performance analysis of MSTES peak-shaving in CFPP

2.1.1. Model construction of MSTES peak-shaving in CFPP

This work takes a typical 600 MW supercritical unit as the object of study, which mainly consists of boiler system, turbine system, feedwater reheat system, and condensing system. The boiler system of this CFPP adopts HG-2070/24.2-HM9 boiler, and the turbine is a primary intermediate reheat single-shaft, three-cylinder, four-exhaust steam turbine with direct air-cooled condensation, with a turbine discharge pressure of

4.5 kPa. The feedwater heating system consists of three high-pressure heaters (HPHs), one deaerator and four low-pressure heaters (LPHs). Coal quality data for the boiler system is shown in Table S1 of supplementary material, and the results of the main parameters of the plant under different operating conditions are shown in Table S2 of supplementary material. In this study, the CFPP coupled heat storage and peak-shaving model is to introduce a molten salt heat storage device in the traditional CFPP, and the change of the power output is realized through the heat exchange between the steam and molten salt to complete the flexibility peak-shaving.

MSTES is the key part of the peak-shaving model to store thermal energy and regulate the unit output, mainly composed of storage, heat release heat exchanger and high and low temperature molten salt tanks, molten salt pumps. The efficiency of the molten salt pump is set at 85 % (based on the average measured value of large centrifugal pumps), with a temperature difference of 5 °C at the heat exchanger end, and an electric heating efficiency of 98 %. Table 1 compares the properties of the two types of molten salts currently mainstream in the market. Compared with Solar Salt (60 % $NaNO_3$ + 40 % KNO_3), Hitec molten salt's (53 % KNO_3 + 7 % $NaNO_3$ + 40 % $NaNO_2$) freezing point is as low as 150 °C, preventing molten salt freezing under a 40 % turbine heat acceptance (THA) load (minimum feedwater temperature of 128 °C), and its decomposition temperature of 535 °C is higher than the design steam extraction temperature of 476 °C [37], which matches well with the temperature range of steam used in 600 MW CFPP peak-shaving [38]. Therefore, the selected molten salt is Hitec molten salt, the superiority of Hitec salt in critical aspects makes it a better solution for peak shaving retrofitting of supercritical power plants. Finally, the design of the system modeling process is shown in Fig. 1.

Assuming that the molten salt in the molten salt tank is fully mixed and the temperatures are equal everywhere, the work mass in the tank follows the following mass and energy conservation equations [39,40]:

$$\frac{dM_t}{dt} = q_{t,i} - q_{t,o} \tag{1}$$

$$\frac{dE_t}{dt} = q_{t,i}c_{p,s}T_{t,i} - q_{t,o}c_{p,s}T_{t,o} - Q_{loss} \tag{2}$$

$$Q_{loss} = k_t A_t\left(T_{t,i} - T_0\right) \tag{3}$$

where M_t, E_t for the molten salt in the tank mass and energy, kg, kJ; $q_{t,i}$, $q_{t,o}$ for the molten salt tank inlet and outlet flow rate, kg/s; $T_{t,i}$, $T_{t,o}$ *and* T_0 are the molten salt tank inlet and outlet temperature of the molten salt and the external ambient temperature, K; Q_{loss} is the external heat dissipation of the molten salt tank, kW; k_t for the coefficient of dissipation of heat, kW/ (m^2·K); At is the area of the heat, m^2.

Assuming that the metal heat storage in the heat exchanger and the molten salt tank and the heat loss of the system piping equipment are ignored in the modeling process, the energy conservation equation for the molten salt side is:

$$M_s c_{p,s}\frac{dT_{s,i}}{d_t} = q_s c_{p,s}\left(T_{s,i} - T_{s,o}\right) + Q_h \tag{4}$$

$$Q_h = A_h\alpha_h\frac{T_{s,o} - T_{s,i}}{\ln\left(\frac{T_s - T_{s,o}}{T_s - T_{s,i}}\right)} \tag{5}$$

Table 1
Comparison of the properties of mainstream molten salts.

Properties	Hitec salt	Solar salt
Operating temperature (℃)	150–535	290–565
Melting point (℃)	142	223
Thermal conductivity (W/(m·K)$^{-4)}$	0.571	0.492
Density(kg/m^3)	2317.5	1924.6
Specific heat capacity/(J·(kg·K)$^{-1}$)	1550	1488

$$\alpha_h = \alpha_{h,0}\left(\frac{q_e}{q_{e,o}}\right)^{0.6} \tag{6}$$

where M_s is the mass of molten salt inside the heat exchanger, kg; $c_{p,s}$ is the specific heat capacity of molten salt, kJ/(kg·K); q_s is the mass flow rate of molten salt through the heat exchanger, kg/s; $T_{s,i}$, $T_{s,o}$ and T_s are the temperature of molten salt in and out of the heat exchanger and the saturation temperature, K; Q_h is the heat exchanger heat transfer, kW; α_h is the heat transfer coefficient, kW/(m^2·K); A_h is the heat transfer area of heat storage heat exchanger, m^2; q_e, $q_{e,0}$ are the actual working condition and design working condition heat exchanger vapor flow rate, kg/s; $\alpha_{h,0}$ is the heat transfer coefficient of heat exchanger under the rated working condition, kW/(m^2·K).

Assuming that the pressure inside the heat exchanger remains constant, the equation of conservation of energy on the tube and shell side is:

$$M_{h,s}c_{p,s}\frac{dT_{hs,o}}{dt} = q_{h,s}c_{p,s}\left(T_{hs,i} - T_{hs,o}\right) - Q_h \tag{7}$$

$$M_{h,w}c_{p,w}\frac{dT_{hw,o}}{dt} = q_{h,w}c_{p,w}\left(T_{hw,i} - T_{hw,o}\right) + Q_h \tag{8}$$

$$Q_h = A_h\alpha_h\frac{\left(T_{hs,i} - T_{hw,o} - T_{hs,o} + T_{hw,i}\right)}{\ln\left(\frac{T_{hs,i} - T_{hw,o}}{T_{hs,o} - T_{hw,i}}\right)} \tag{9}$$

where M_{hs}, M_{hw} for the heat exchanger salt, feed water mass, kg; $q_{h,s}$, $q_{h,w}$ for the heat exchanger salt and feed water flow rate, kg/s; $T_{hs,i}$, $T_{hs,o}$ and $T_{hw,i}$, $T_{hw,o}$ are heat exchanger inlet and outlet temperature of the molten salt and feed water temperature, K; Q_h for the heat exchanger heat transfer, kW; $c_{p,\,w}$ for the specific heat capacity of feed water, kJ / (kg·K); A_h is the heat transfer area in the heater, m^2; α_h is the heat transfer coefficient of the heater, kW/(m^2·K).

Through comprehensive comparison, it is found that when MSTES selects reheat steam to heat the low-temperature molten salt, and the heated steam enters the outlet of the deaerator, and the molten salt heat release scheme selects the high-temperature molten salt to heat the outlet water of the feedwater pump, and the heated water enters into the boiler feed water in the way of the highest comprehensive peak-shaving performance [27,41]. Therefore, this study designs the coupling system for peak-shaving by this scheme and builds the model by Ebsilon. Ebsilon is a professional thermal system simulation software, with its modular modeling capability and accurate thermodynamic algorithms, it shows significant advantages in the simulation of peak-shaving of coal-fired units. The software can efficiently construct complex unit models, flexibly simulate the dynamic characteristics of boilers, turbines and other key equipment under different load conditions, accurately quantify the trends of efficiency, energy consumption and emission parameters during low-load operation, and support rapid adjustment of operation strategies to optimize the economics of peak-shaving.

The specific modeling process is as follows. Firstly, the inlet pressure of the high-pressure cylinder is set in the EBSILON to be externally given, i.e., by the boiler, which facilitates the sliding pressure operation at variable loads. The inlet pressure of the turbine at all levels is set according to the pressure on the heat balance diagram, and the pressure of the turbine under variable load is set according to the Ferrigal formula. The main parameters of the peak-shaving model are shown in Tables S1–S2 of the supplemental material.

The final model constructed is shown in Fig. 2. The verification of the model is shown in Table S3 of the supplemental material, where it can be found that the main steam pressure has the largest error, reaching 0.92 %, while the main steam temperature has the smallest error, only 0.05 %, so the errors of the model are all within 2 %, indicating the reliability of the model.

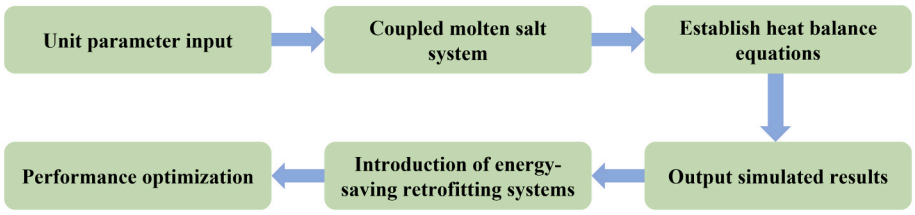

Fig. 1. Modeling approach for coal-fired power plant coupled molten salt thermal energy storage peak shaving with energy-saving retrofitting technology.

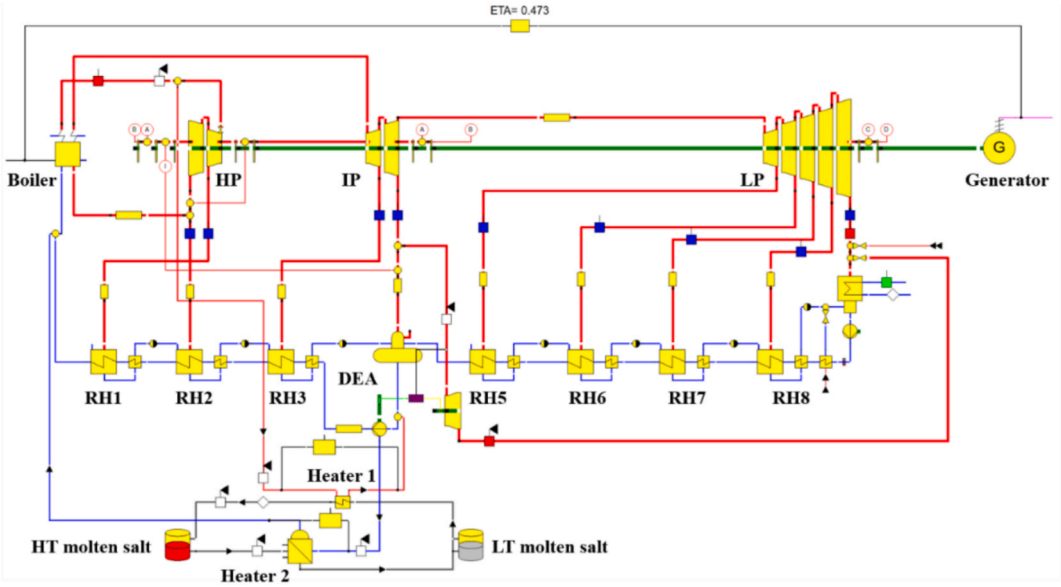

Fig. 2. Modelling of 600 MW supercritical plant coupled with molten salt heat storage.

2.1.2. Performance analysis of MSTES peak-shaving in CFPP

The performance of peak-shaving at this time can be obtained through simulation calculations as shown in Table 2. It can be observed that the peak shaving capacity of coal-fired power plants utilizing coupled molten salt thermal energy storage has been significantly enhanced, thereby validating the feasibility of this peak shaving scheme.

Furthermore, the heat storage and release capacity of the molten salt device is particularly important for the entire peak shaving process. Therefore, it is necessary to consider the full load operating time and cycle number of the molten salt system during heat storage and release, and evaluate its availability during continuous peak shaving.

The peak shaving capacity of a molten salt thermal storage system is determined by the heat storage and release capacity and dynamic response characteristics, and the formula for calculating the duration of a single peak load adjustment is:

$$t = \frac{m \times C_p \times \Delta T \times \eta}{P_{peak}} \tag{10}$$

Table 2
Peak-shaving performance of 600 MW supercritical CFPP peak-shaving model.

Parameters	Heat storage	Heat release	Heat storage and release
Power generation (MW)	214.81	634.06	214.81–634.06
Heat storage load (MW)	60.000	60.000	60.000
Peak-shaving capacity (MW)	25.73	31.31	57.04
Peak-shaving depth (%)	4.29	5.19	9.51
Thermoelectricity conversion efficiency (%)	42.88	52.18	47.53
Thermal efficiency (%)	38.57	41.83	40.52
Exergy efficiency (%)	37.54	40.49	39.31

Where m is the mass of molten salt, C_p is the specific heat capacity of molten salt of 1.56kJ/(kg·K), ΔT is the temperature rise during operation, η is the system efficiency (typically 92 %), and P_{peak} is the peak shaving load.

Calculating by the above formula, the peak shaving duration for the heat storage process is 1.63 h, and the daily peak shaving duration for the heat release process is 1.18 h, resulting in a total cycle time of 2.81 h. Assuming that the peak shaving duration for a coal-fired power plant is 8 h and the plant operates for 300 days per year, the annual cycle count for the coupled system is approximately 854 cycles. The mass flow in the molten salt system is 2,860 t/h, and the annual loss rate of Hitec salt is 1.8 %, resulting in an annual molten salt loss of 123,500 tons. Through calculation, it can be seen that the peak shaving capacity of the coal-fired power plant coupled with molten salt thermal storage meets the peak shaving requirements of a typical power plant, thereby demonstrating the feasibility of the coupled system.

The comparison of the coal consumption before and after peak-shaving is shown in Table 3. It can be found that the coal consumption of the system after peak-shaving is much higher than that of the initial model without MSTES. As a result, the overall thermal cycle of the system and the main engine equipment will run away from the design

Table 3
Comparison of coal consumption before and after peak-shaving of 600 MW supercritical CFPP.

Parameters	Peak-shaving process	Initial process
Unit heat consumption rate (kJ/kWh)	7896.50	7687.36
Coal consumption for power supply (g/kWh)	310.37	300.97

conditions while working at partial load, which will affect the economics of operation. In order to reduce the coal consumption of the peak-shaving model and improve the economy of the peak-shaving model during low-load operation, energy-saving modifications are needed for the low load operation of the peak-shaving model.

The turbine of the 600 MW supercritical CFPP is designed for slip-pressure operation, which enables the turbine to maintain high efficiency over a wide range of load variations, especially since its relative internal efficiency is still not lower than the design working condition during low-load operation. Therefore, the reduction of the low-load operation economy is less related to the turbine parameter changes and mainly originates from the increase of the unit heat consumption rate caused by the reduction of the boiler feed water temperature and the initial parameters of the cycle. At this time, if certain modification measures are taken, the final feedwater temperature can be increased when it's in low-load operation, improving the thermal economy of the peak-shaving system's operation. Considering the factors such as not affecting the efficiency of the original system, the complexity of equipment arrangement, and the cost of new equipment, the front steam cooler (FSC) and No. 0 high-pressure heater (HPH) can be adopted to carry out energy-saving modification of the peak-shaving system.

2.2. Energy-saving retrofit scheme design – Front steam cooler (FSC)

Table 4 shows the parameters of all levels of steam extraction of 600 MW CFPP, it can be seen that the superheat of all levels of extracted steam after reheating steam of the CFPP is large, especially the superheat of the third level of extracted steam is the largest, which has been higher than 250℃, resulting in a large difference in the heat transfer temperature of the corresponding No. 3 HPH, which has caused a large irreversible loss. Therefore, in order to minimize the heat loss and reduce the energy consumption of the system, it is necessary to reduce the heat transfer temperature difference of the No. 3 HPH. The addition of a FSC in front of the No. 3 HPH is an effective way to reduce the heat transfer temperature difference of the heater [36]. According to the second law of thermodynamics, the smaller the heat transfer temperature difference is, the smaller the irreversible loss is. Therefore, to improve the thermal economy of the FSC, the superheat of the third-stage extracted steam should be applied as much as possible to the last-stage HPH, which is the rear end of the No. 1 HPH, the front end of the boiler feedwater, and the feedwater flow to the boiler after the heat exchange.

This method reduces superheat of the third-stage extracted steam and reduces the heat transfer temperature difference, thus reducing the irreversible loss, while utilizing the superheat of the third-stage extracted steam to heat the No. 1 HPH outlet feedwater, raising the temperature of the boiler feedwater, reducing the boiler's heat loss, and

Table 4
Parameters of steam extraction at all levels of 600 MW supercritical CFPP.

Parameters	Pressure (MPa)	Temperature (℃)	Saturation temperature (℃)	Overheating (℃)
1st-stage steam extraction	6.10	358.93	276.71	82.22
2nd-stage steam extraction	4.08	309.14	251.32	57.82
3rd-stage steam extraction	2.16	476.12	216.10	260.02
4th-stage steam extraction	1.07	370.65	182.95	187.7
5th-stage steam extraction	0.47	269.68	149.55	120.13
6th-stage steam extraction	0.13	140.84	107.14	33.7
7th-stage steam extraction	0.06	86.54	85.95	0.59
8th-stage steam extraction	0.02	60.52	60.06	0.46

effectively improving the thermal economy of the peak-shaving unit. As an independent heat exchanger to complete the heating task, due to the complexity of the system, equipment and piping investment is larger, the heat return system is mostly used only 1 FSC to guarantee the requirements of economy.

FSC is mainly connected in tandem and parallel connection mode, connection mode is different from its thermal economic effect there are also big differences. Among them, the tandem-connected FSC is divided into two types of full-capacity and partial-capacity tandem-connected, as shown in Fig. 3. The full-capacity structure of the FSC is set at the outlet of the No. 1 HPH, which is connected to the No. 1 HPH export feed water pipeline, and utilizes the third-stage extraction of steam from the turbine to heat up all the feed water. At this time, the inlet water has a high temperature, the average temperature difference of the heat transfer process is relatively small, and the extraction of steam is more adequately utilized for the degree of superheat. The difference between the partial-capacity and the full-capacity structure is that a bypass gate is added, and the heated medium is part of the feed water.

In this study, 40 % THA (Turbine Heat Acceptance) and 100 % THA are selected as the molten salt heat storage and heat release process conditions, respectively. When the FSC is partially arranged in tandem, the comparison of boiler outlet feedwater temperature and heat rate for power supply under different operating conditions with different diversion ratios R (ratio of feedwater flowing into the FSC to the total feedwater flow rate) is shown in Fig. 4, when R = 0, the feedwater from No. 1 HPH doesn't flow through the FSC, and flows directly to the boiler; when R = 1.0, the FSC is arranged in tandem, and all the feedwater from No. 1 HPH flows through the FSC. It is found that as the R increases, the boiler feedwater temperature increases and the overall unit heat consumption rate decreases. Therefore, the FSC selection of full-capacity tandem-connected is more effective. This not only reduces the heat transfer temperature difference between the two, but also reduces the superheat of the No. 3 steam extraction, thus reducing the thermal system losses.

The structure of the parallel arrangement of FSC is shown in Fig. 5. The FSC is arranged in parallel with the No. 1 HPH, and the third-stage steam extraction and the No. 1 HPH jointly heats the feedwater. The boiler outlet feedwater temperature and heat rate for power supply of different R under the parallel structure of the FSC under different working conditions of are shown in Fig. 5. When R = 0, all the feedwater from No. 2 HPH flows into No. 1 HPH, without flowing into the FSC, which is the same as that in Fig. 4 with R = 0 condition; when R = 1, all the feedwater from No. 2 HPH flows into the FSC, without flowing into No. 1 HPH. From Fig. 6, with the increase of the R, the boiler feedwater temperature decreases, the unit heat consumption rate increases, and the thermal economy is poor. This is due to the parallel FSC although it can relatively reduce the feedwater resistance, its feedwater temperature is low, the heat transfer temperature difference is large, and at the same time the feedwater diversion into the next level of the main feedwater flow is reduced, the corresponding extraction mass flow is reduced, resulting in a relatively low thermal economy.

In summary, based on the above simulation results of different arrangements of FSC, in order to minimize the superheat of the third-stage steam extraction, enhance the boiler feedwater temperature, and consider the external cooler volume, cost and other factors, the final choice of tandem full-capacity FSC. At this time, all of the No. 1 HPH outlet feedwater enters the FSC, and the feedwater after heat exchange then enters the boiler economizer. The final model of energy-saving modification of CFPP coupled with MSTES is shown in Fig. 7.

2.3. Energy-saving retrofit scheme design – No. 0 high-pressure heater (HPH)

When the system operates under low load conditions, the turbine exhaust steam temperature and pressure are low, and the original HPHs of the CFPP are unable to effectively utilize the exhaust steam waste

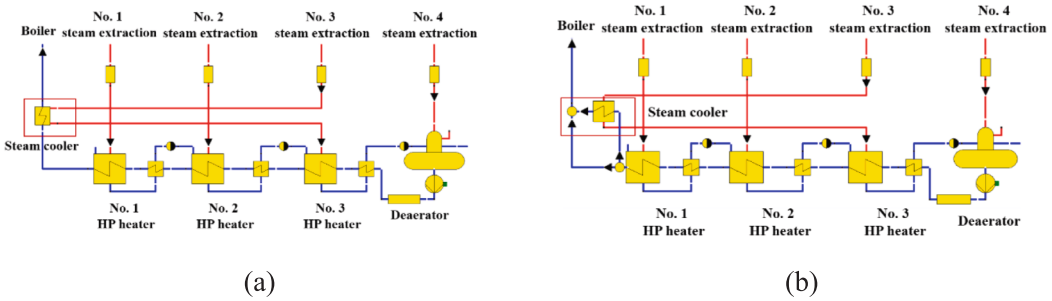

Fig. 3. FSC tandem scheme design: (a) full-capacity tandem structure; (b) partial-capacity tandem structure.

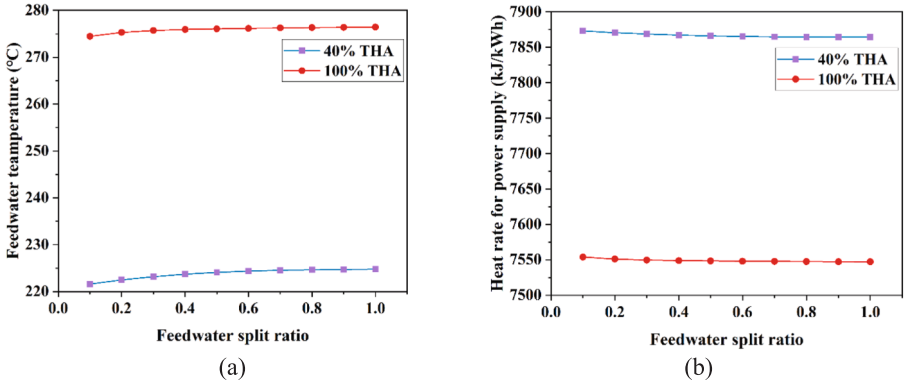

Fig. 4. Comparison of parameters with different R for the FSC in tandem scheme: (a) outlet feedwater temperature; (b) the unit heat consumption rate.

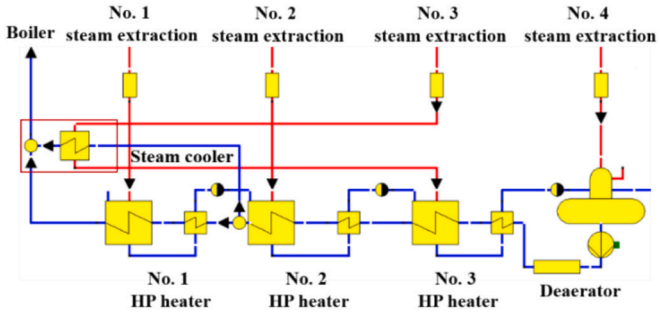

Fig. 5. FSC parallel-connected scheme design.

heat, which will result in additional losses in the thermal cycle. In order to solve this problem, it is necessary to improve the utilization efficiency of turbine exhaust waste heat. Therefore, it is possible to set up an additional No. 0 HPH in front of the No. 1 HPH of the system's feedwater reheat system, which is operated in series with the original three HPHs, and share the feedwater bypass of the original feedwater system [35]. At this time, the SEPP is arranged in the steam guide of the high-pressure cylinder make-up valve, so that the high-pressure cylinder steam is led out to be used as a heating source of No. HPH. This method not only makes full use of the exhaust heat of the turbine, but also further improves the efficiency of feedwater heat, reduces the heat absorption of the feedwater in the boiler system and the coal consumption of the peak-shaving system, and improves the thermal economy of the peak-shaving system.

The introduction of the No. 0 HPH technology can improve the adaptability of the peak-shaving system to load fluctuations and improve the flexibility of the overall system. The parameter settings of

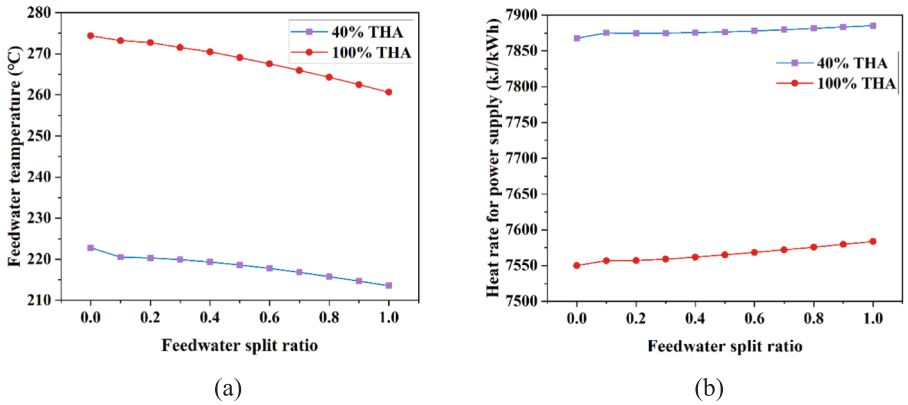

Fig. 6. Comparison of parameters with different R for the FSC in parallel scheme: (a) outlet feedwater temperature; (b) the unit heat consumption rate.

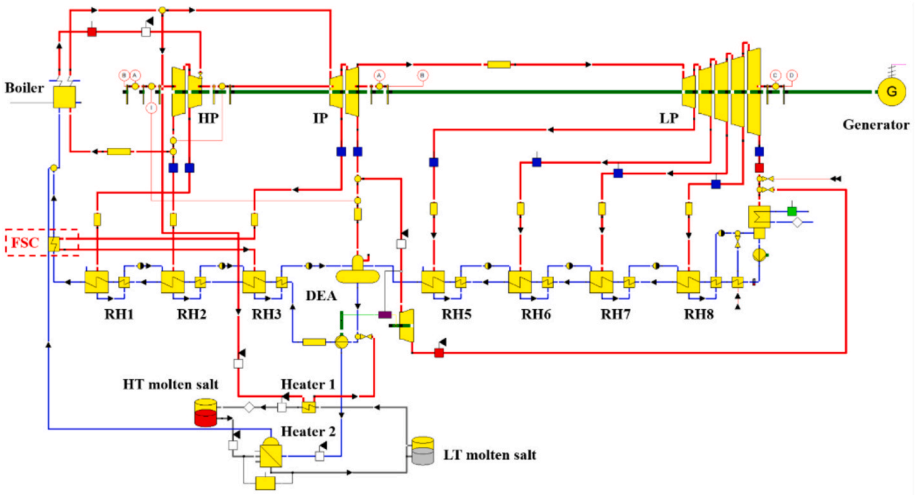

Fig. 7. Energy-saving retrofit model coupled with FSC of 600 MW CFPP with molten salt heat storage for peak-shaving.

the No. 0 HPH refer to the original No. 1 HPH, and the upper difference of the No. 0 HPH is set to −1.7℃, the lower difference is set to 5.6℃, and the pumping pipeline pressure loss is set to 3.0 %. Meanwhile, the boiler feedwater temperature is guaranteed to be no more than 320 °C during the simulation process to ensure the stability and safety of the boiler operation. The No. 0 HPH is connected in two ways: full-capacity and partial-capacity tandem connection, as shown in Fig. 8.

The boiler outlet feedwater temperature and heat rate for power supply changes of the tandem connection under different diversion ratio R (ratio of inflow of the No. 0 HPH feedwater to total feedwater flow) are shown in Fig. 9. When R = 0, the outlet feedwater of No. 1 HPH flows directly into the boiler in its entirety; when R = 1.0, the outlet feedwater of No. 1 HPH flows into No. 0 HPH in its entirety before flowing into the boiler.

It can be seen that with the increase of the R, the feedwater flowing into the No. 0 HPH increases, the outlet feedwater is further heated, which leads to the outlet feedwater temperature increasing, and the unit heat consumption rate decreases, the thermal economy improves, so when R = 1.0, the No. 0 HPH takes the full-capacity tandem coupling with the best energy-saving effect. At this time, the coupling system is shown in Fig. 10.

3. Optimization of energy-saving retrofit coupling scheme design and peak performance assessment

3.1. Design of energy-saving retrofit coupling scheme

In order to further increase the energy savings of the peak-shaving system, the FSC and No. 0 HPH can be combined to construct an energy-saving modification coupling model for the peak-shaving system. According to the above analysis and the characteristics of the FSC and the No. 0 HPH, the coupling arrangement of the two types of equipment can be arranged in tandem and parallel, as shown in Fig. 11, the No. 0 HPH is arranged downstream of the No. 1 HPH and upstream of the FSC in tandem. The feedwater first enters the No. 0 HPH with a relatively low heat source temperature, then flows to the FSC with a relatively high heat source temperature. In a parallel connection, the FSC is connected in parallel with No. 0 HPH, and the feedwater from No. 0 HPH enters both devices at the same time, and the heat exchanged feedwater enters the boiler.

In order to quantitatively analyze the additional losses that may be incurred by a coal-fired power plant when two energy-saving devices are connected in series or in parallel, this study will calculate the heat loss and resistance effects under different structures by simulation result and relevant formulas. The formulas are as follows:

$$E_{xloss} = T_0 \times m_{salt} \times c_p \times \ln\frac{T_{out}}{T_{in}} \tag{11}$$

$$\Delta\eta_{turbine} = \frac{\Delta W_{pump}}{W_{net}} \times 100\% \tag{12}$$

From Table 5, it can be observed that the parallel structure results in increased heat transfer temperature differences due to water diversion, leading to an 86.8 % increase in irreversible heat loss;while the series structure, although introducing a pipeline resistance of 0.25 MPa, only affects turbine efficiency by 0.12 %. The thermodynamic benefits significantly outweigh the resistance losses, ultimately achieving a net coal consumption reduction of 5.8 g/kWh, thereby validating the comprehensive superiority of the series configuration in engineering applications.

To further analyze the impact of series and parallel structures on the system, Fig. 12 shows the variation of unit parameters for different diversion ratios R (ratio of feedwater flow into the FSC to the total feedwater flow) for the two energy-saving methods arranged in tandem

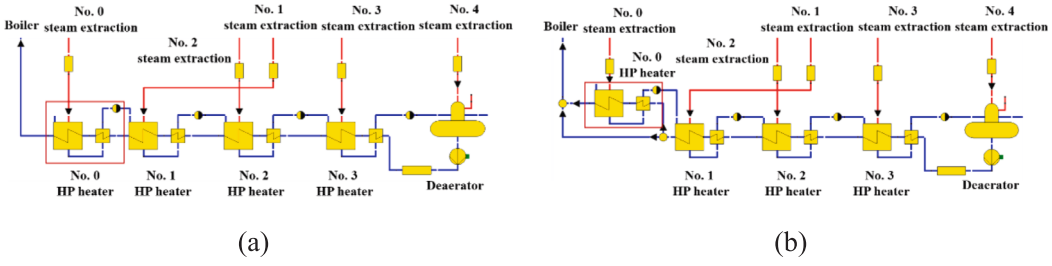

Fig. 8. Schemes of different arrangements of No. 0 HPH: (a) full-capacity tandem structure; (b) partial-capacity tandem structure.

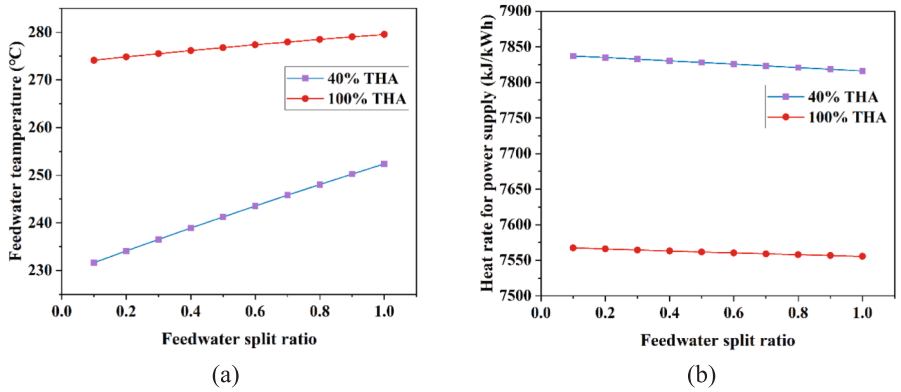

Fig. 9. Parameters comparison of different R for the No. 0 HPH with partial tandem scheme: (a) outlet feedwater temperature; (b) the unit heat consumption rate.

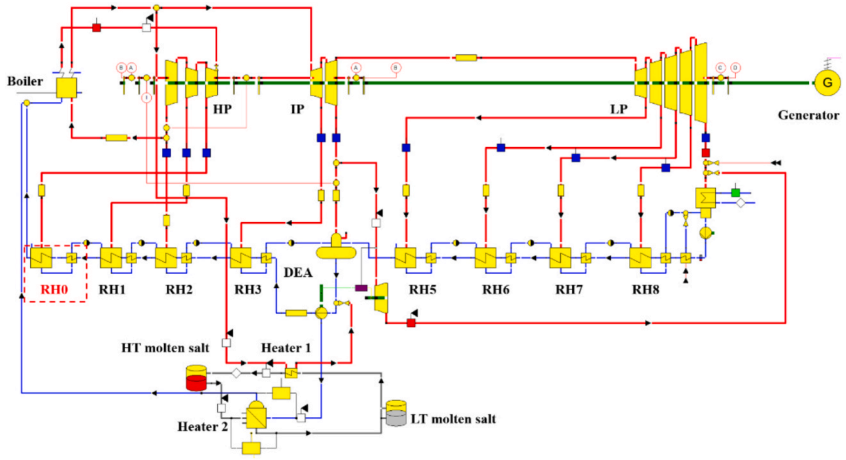

Fig. 10. Energy-saving retrofit model coupled with No. 0 HPH of 600 MW CFPP with molten salt heat storage for peak-shaving.

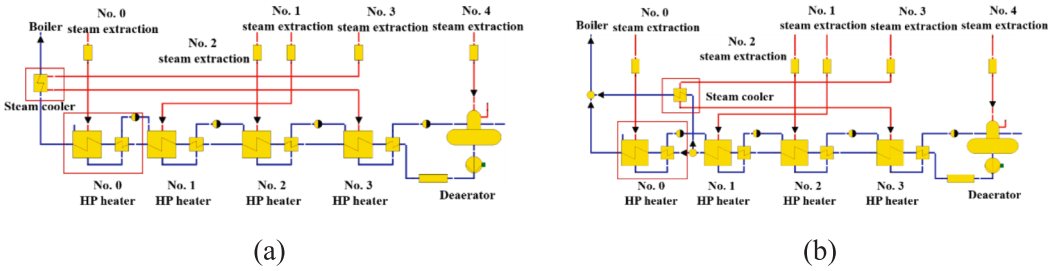

Fig. 11. Design of the coupling arrangement scheme for the FSC and No. 0 HPH: (a) tandem structure; (b) parallel structure.

Table 5
The effect of FSC and No. 0 HPH series–parallel coupling on coal-fired power plants.

Parameters	Series connection	Parrallel connection
Effective heat transfer (MW)	58.2	54.7
Irreversible loss (MW)	3.8	7.3
Exergy efficiency (%)	94.2	88.3
Feedwater system pressure drop (MPa)	1.82	2.07

and parallel. It can be found that as the R increases, the boiler feedwater temperature decreases and the overall unit heat consumption rate increases. Therefore, to increase the boiler feedwater temperature as much as possible and reduce the unit heat consumption rate, it is more effective to connect the FSC and No. 0 HPH in tandem. At this time, not only can reduce the degree of superheat of No. 3 steam extraction to reduce the heat loss of superheated steam, but also increase the boiler feedwater temperature, reduce the heat absorption of feedwater in the boiler system, and further reduce the amount of coal consumption in the peak-shaving system. Additionally, the feedwater temperature of the unit at 40 % THA is 252.3℃, and the unit heat consumption rate is 7805.15 kJ/kWh; The feedwater temperature of the unit at 100 % THA is 282.46℃, and the rate of heat consumption of the power supply is 7545.62 kJ/kWh.

3.2. Sensitivity analysis of energy savings from heat storage and release processes

In order to further reduce the energy consumption of the system, the energy-saving effects of the FSC and the addition of No. 0 HPH on the

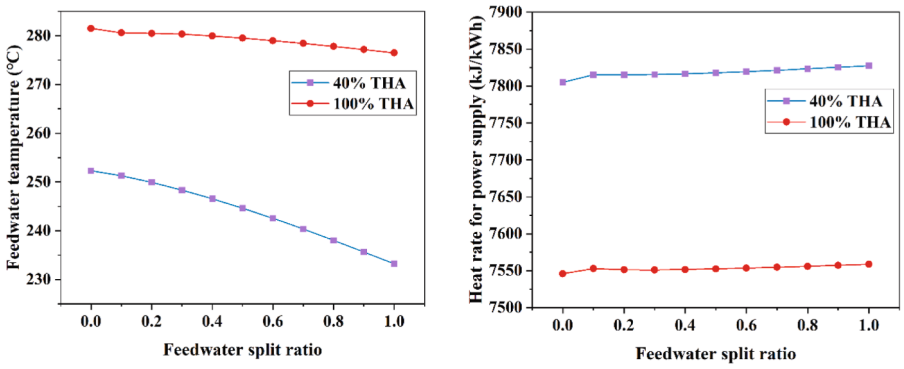

Fig. 12. Parameters comparison of different R for two energy-saving methods by different arrangements: (a) outlet feedwater temperature; (b) the unit heat consumption rate.

CFPP coupled with the MSTES under different operating conditions are comprehensively analyzed in the following. The simulated peak-shaving model built by combining the two energy-saving methods is shown in Fig. 13.

The parameters of the heat storage and release process in the tandem arrangement under the initial parameters are shown in Table 6. It is found that the unit heat consumption rate and coal consumption rate do decrease after the retrofit, and the thermal efficiency and the exergy efficiency are improved, indicating that the peak-shaving model after the introduction of the energy-saving method has better economic benefits and power generation efficiency compared with the model without energy-saving retrofit. In supercritical CFPPs, since the turbine is operated at slip pressure, the turbine extraction pressure decreases as the unit load decreases, which restricts the improvement of the overall thermal cycle efficiency of the system. After introducing energy-saving retrofitting technology, the boiler efficiency of the peak load model's heat storage and release process was also improved accordingly.

The various levels of heaters and the various levels of turbine steam extraction are usually one-to-one correspondence, and the different inlet steam parameters will affect the thermal economy of the unit. In addition, the return heat efficiency of the return heat system of feedwater is inseparable from the feedwater temperature. Therefore, in order to further investigate the influence of different parameter changes on energy saving and obtain the best solution, the following will analyze and optimize the steam inlet parameters of No. 0 HPH and the boiler feedwater temperature changes on the coal consumption parameters such as

Table 6
The main parameters of the coupled system combining the two energy-saving methods in tandem under different operating conditions.

Parameters	Before energy-saving retrofit (40 % THA)	After energy-saving retrofit (40 % THA)	Before energy-saving retrofit (100 % THA)	After energy-saving retrofit (100 % THA)
Unit heat consumption rate (kJ/kWh)	7839.37	7805.15	7557.6	7545.6
Coal consumption for power supply (g/kWh)	307.46	306.12	297.74	296.42
Overheating of 3rd-stage steam extraction (℃)	260.02	74.51	186.37	58.46
Thermal efficiency (%)	38.91	39.68	41.16	41.51
Exergy efficiency (%)	37.83	38.74	39.90	40.24
Boiler efficiency (%)	92.80	93.43	93.25	93.56
Power generation (MW)	241.57	231.04	602.59	598.92
Feedwater outlet temperature (℃)	229.14	252.3	273.32	282.46

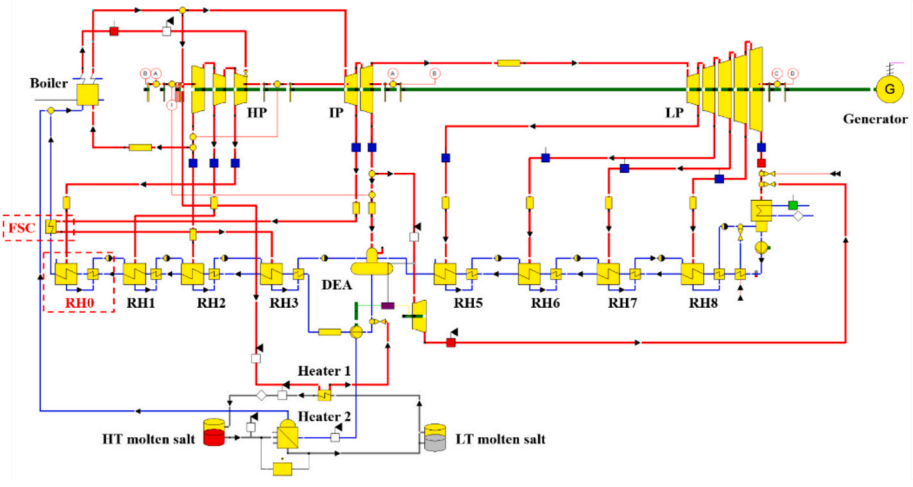

Fig. 13. Energy-saving retrofit model coupled with FSC and No. 0 HPH of 600 MW CFPP with molten salt heat storage for peak-shaving.

unit heat consumption rate of before and after the addition of the energy-saving measures in the peak-shaving model, respectively.

3.2.1. Influence of feedwater temperature variation and the unit heat consumption rate at different SEPPs during heat storage process

Considering the design parameters of the HPH and the limitations of the boiler feedwater temperature, a regulating valve is set up on the No. 0 extractor pipeline. The inlet steam pressure of the No. 0 HPH can be controlled by adjusting the opening of the regulating valve on the No. 0 section of the extractor pipeline in different working conditions, which affects the heat exchange between the extractor and the feedwater, and then adjusting the temperature of the No. 0 HPH outlet water, to control the temperature of the feedwater that enters the coal economizer of the boiler. In order to ensure the reliability of the analysis, the total amount of air on the furnace side, coal input, and the main steam flow rate are kept constant at the corresponding load [42]. In addition, in order not to cause boiler overheating, water-cooled wall piping deformation and other problems, it is necessary to ensure that the feedwater temperature does not exceed 320 ℃ when it is increased [43].

In the heat storage process, under the determined SEPP, adjust the regulating valve opening behind the 0-stage steam extraction to control the boiler feed water temperature, and then get the boiler feed water temperature and the unit heat consumption rate under different SEPP, as shown in Fig. 14. At this time, setting the position of the 0-section extraction pressure to start from 3 MPa and increase according to the 0.5 MPa incremental rate up to 7.5 MPa, and the dotted line is the unit heat consumption rate when energy-saving methods have not been added. The dotted line in the figure is the unit heat consumption rate without adding energy-saving equipment. It can be found that when the boiler feedwater temperature is the same, with the increase of the pressure at the SEPP, the unit heat consumption rate of the unit increases. The reason is that the steam extraction occurs in the turbine high-pressure cylinder at a more forward position, the high-pressure steam is not fully expanded, and a part of the thermal energy that can be converted into mechanical energy is lost, and the effective power output from the high-pressure cylinder decreases, and the heat consumption of the unit increases.

At the same SEPP, when the pressure at the SEPP is less than 6 MPa (located at the rear end of the high-pressure cylinder), with the increase of feedwater temperature, the rate of heat consumption decreases, and almost all of them are lower than the unit heat consumption rate when energy-saving retrofit equipment is not added. The reason is that the effective enthalpy drop of steam before the exhaust steam port is small, and the economic improvement brought by using high-pressure steam extraction to heat the feedwater is greater than the reduction of the economy brought by the work done by the high-pressure steam extraction less in the turbine. At this time, there is a minimum value of the heat consumption rate, marked with a hollow pentagram in Fig. 14. The reason for the existence of the minimum value is that when the boiler feed water temperature increases, the heat absorption of the work material in the boiler decreases but makes the unit heat consumption rate increase, and both of them affect the unit heat consumption rate at the same time, so there is bound to be a minimum value in the interval;

When the pressure at the SEPP is greater than 6 MPa (located at the front end of the high-pressure cylinder), with the increase in feed water temperature, the unit heat consumption rate rises. This is because the effective enthalpy drop of steam before the exhaust port is significantly increased, and the economic improvement brought by using high-pressure steam extraction to heat the feedwater under the same load is smaller than the economic reduction brought by the less work done by high-pressure steam extraction in the turbine.

Ultimately, the optimum value for energy saving and transformation of the heat storage process can be obtained, which is the position marked by the solid pentagram in Fig. 14. The corresponding extraction pressure is the optimum 0-stage extraction pressure, and the corresponding unit heat consumption rate at this time is the optimum heat consumption rate. When it is lower than the optimal 0-stage extraction pressure, as the extraction pressure decreases, the heat consumption rate gain of the unit decreases. This is because in the operation of the No. 0 HPH, with the decrease of the 0-stage extraction pressure, the temperature rise of the boiler feedwater can decrease, and the average heat-absorbing temperature of the feedwater decreases; When it is higher than the optimal 0-stage extraction pressure, with the increase of the 0-stage extraction pressure, the heat consumption rate gain of the unit decreases. This is because when the No. 0 HPH is put into operation, the steam quality gradually increases with the increase of the 0-stage extraction pressure, and the unit heat consumption rate gains since the use of high-quality steam for reheating is gradually smaller than the loss caused by the reduction of work done. Finally, the optimal 0-stage extraction pressure is 4 MPa, the boiler feedwater temperature is 258.14℃, and the optimal unit heat consumption rate is 7744.84 kJ/kWh.

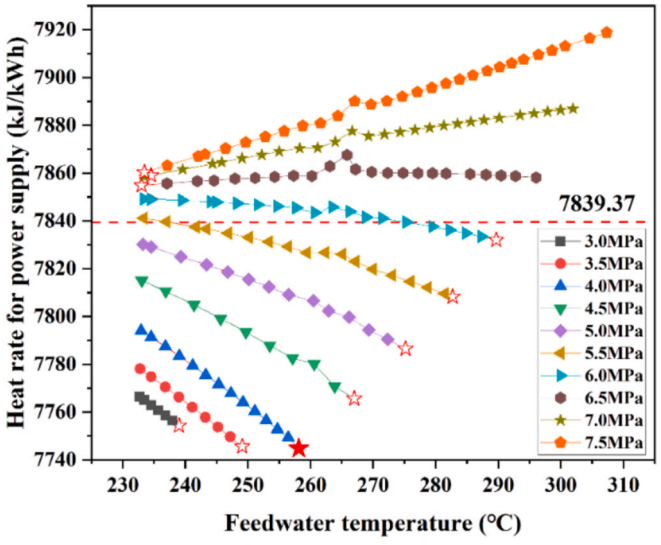

Fig. 14. Boiler feedwater temperature and unit heat consumption rate at different SEPPs for heat storage process after coupling energy-saving equipment.

3.2.2. Influence of feedwater temperature variation and the unit heat consumption rate at different SEPPs during heat release process

In the heat release process, the boiler feedwater temperature and the unit heat consumption rate under different SEPPs are shown in Fig. 15, and the 0-stage extraction pressure is set to start from 7 MPa and increase to 15 MPa in accordance with the 1.0 MPa growth rate. It can be found that when the boiler feedwater temperature is the same, the unit heat consumption rate rises as the SEPP pressure rises for the same reason as the heat storage process. At the same SEPP, when the pressure at the SEPP is less than 14 MPa, as the feedwater temperature increases, the unit heat consumption rate decreases. The reason is that the increase in the economy brought about by using high-pressure steam extraction to heat the feedwater is greater than the decrease in economy brought about by the less work done by the high-pressure steam extraction in the turbine. But it cannot keep increasing the feedwater temperature in one way or the other. Because the increase in feedwater temperature will be limited by some of the materials used in the boiler economizer and other parts of the boiler, and when the temperature is higher than 320 °C, material replacement costs increase significantly.

Therefore, for a certain inlet pressure, there exists a corresponding optimal feedwater temperature to maximize the thermal efficiency of the unit, and there is also a minimum value of the unit heat consumption rate, which is marked by a hollow pentagram in Fig. 15. The existence of extreme value is for the same reason as the heat storage process. When the pressure at the SEPP is greater than 14 MPa, the unit heat

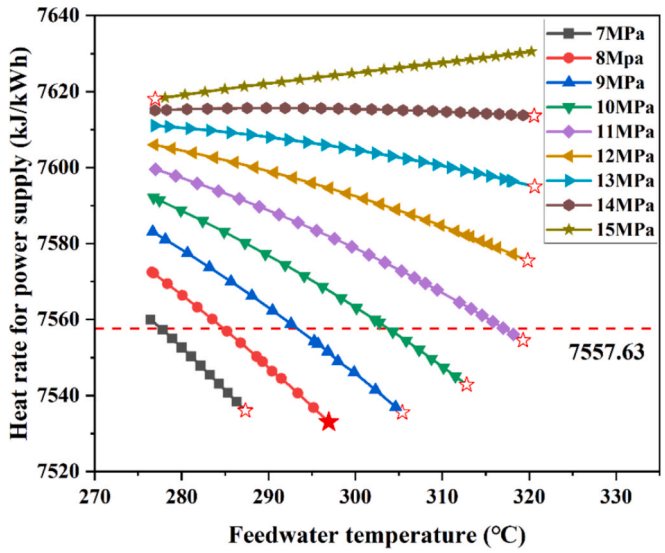

Fig. 15. Boiler feedwater temperature and unit heat consumption rate at different SEPPs for heat storage process after coupling energy-saving equipment.

consumption rate increases as the feedwater temperature rises. This is because the increase in economy brought about by using high-pressure steam extraction to heat the feedwater at the same load is less than the decrease in economy brought about by the less work done by the high-pressure steam extraction in the turbine. Finally, the optimum value for the energy-saving modification of the heat storage process can be obtained. The position is marked by the solid pentagram in Fig. 15, at which the optimum 0-stage extraction pressure is 8 MPa, the boiler feedwater temperature is 296.94 °C, and the optimum unit heat consumption rate is 7533.01 kJ/kWh.

Finally, the comparison of the main performance parameters of the peak-shaving model before and after the optimization of the SEPP is shown in Table 7. The power consumption of auxiliary equipment such as molten salt pumps and electric heaters is 5.59 MW. This energy consumption must be taken into account when calculating the energy consumption of the renovated system. After optimization, the unit heat consumption rate can be reduced by up to 60.31 kJ/kWh in the heat storage process, and the coal consumption for power supply can be reduced by up to 2.19 g/kWh, at which time the boiler feedwater temperature rises by 6.84℃; The unit heat consumption rate can be reduced by up to 12.61 kJ/kWh in the heat release process, and the coal consumption for power supply can be reduced by up to 1.85 g/kWh, at which time the feedwater temperature rises by 14.48℃.

3.3. Performance analysis of peak-shaving model after energy-saving retrofit

After the introduction of the FSC and No. 0 HPH, the coal consumption of the peak-shaving unit is greatly reduced, which improves the thermal economy of the peak-shaving model. However, the peak-shaving performance of the retrofitted peak-shaving model is also very important, which is related to the ability to regulate the load variation range of the whole coupled model.

Therefore, in order to analyze the performance of the energy-saving retrofitted peak-shaving model, the following calculations and analyses will be carried out for the peak-shaving performance (mainly including the peak-shaving capacity, peak-shaving depth, etc.) and thermodynamic performance (coal consumption for power supply, thermal efficiency, exergy efficiency, thermoelectric conversion efficiency, etc.) of the retrofitted peak-shaving model, and the calculation formulas for various types of peak-shaving performance indicators are shown in Table S4 of the Supplementary material [21,44].

The peak performance of the heat storage process and release process before and after the retrofit is obtained through the detailed calculation formulae, as shown in Table 8, in which the unit generating output at 40 % load before peak-shaving is 240.53 MW, and the initial generation output at 100 % is 602.60 MW.

During the heat storage process, the peak-shaving performance of the modified model is better than that of the peak-shaving model before the modification. The reason is that during the heat storage process, the introduction of the FSC and the No. 0 HPH will increase the boiler feedwater temperature, which will improve the quality of the boiler's main steam and reheat steam, making the MSTES able to absorb more heat, which in turn will further reduce the unit's power output and improve the peak-shaving performance. At the same time, due to the increase in feedwater temperature and the efficient utilization of extracted steam waste heat, the heat loss of the boiler and heat transfer temperature difference of the steam turbine extracted steam are reduced, and the thermal efficiency and efficiency of the unit are improved. In addition, due to the introduction of energy-saving equipment, the coal consumption of the peak-shaving model is significantly reduced, and the unit heat consumption rate is reduced by 94.53 kJ/kWh.

In the heat release process, the retrofitted model exhibits superior peak-shaving performance compared to the pre-retrofit system. The reason is that the introduction of the energy-saving equipment makes the boiler feedwater temperature match the feedwater temperature of the high-temperature molten salt heat exchange more closely, thus increasing the unit output and improving the peak-shaving

Table 8
Peak-shaving performance of heat storage process and release process before and after energy-saving retrofit.

Parameters	Heat storage		Heat release	
	Before retrofit	After retrofit	Before retrofit	After retrofit
Power generation (MW)	231.83	230.97	613.04	616.33
Unit heat consumption rate (kJ/kWh)	7839.37	7744.84	7557.63	7533.01
Heat storage load (MW)	20.00	20.00	20.00	20.00
Peak-shaving capacity (MW)	8.70	9.56	10.44	13.73
Peak-shaving depth (%)	1.44	1.59	1.73	2.54
Thermoelectric conversion efficiency (%)	43.50	47.80	52.20	68.65
Thermal efficiency (%)	38.91	41.28	41.16	41.55
Exergy efficiency (%)	37.83	38.83	39.90	40.86

Table 7
Comparison of the main performance parameters before and after optimization of SEPP to the heat storage and release process.

Parameters	Heat storage process		Change value	Heat release process		Change value
	Before optimization	After optimization		Before optimization	After optimization	
Extraction port location (MPa)	4.00	4.00	–	8.00	8.00	–
Unit heat consumption rate(kJ/kWh)	7805.15	7744.84	60.31	7545.62	7533.01	12.61
Coal consumption for power supply (g/kWh)	306.12	303.93	2.37	296.42	294.57	1.97
Feedwater temperature (°C)	252.30	259.14	6.84	282.46	296.94	14.48

performance. At this time, the energy loss is smaller, and the thermal efficiency and exergy efficiency are both improved. Also due to the introduction of energy-saving equipment, the coal consumption of the peak-shaving model is significantly reduced, the unit heat consumption rate is reduced by 24.62 kJ/kWh. Therefore, the energy-saving reformed peak-shaving model not only reduces the coal consumption of the unit, but also improves the peak-shaving performance of the unit, which can provide a guide to the subsequent optimization of peak-shaving of coal-fired units.

3.4. Analysis of the applicability and stability after energy-saving retrofit

3.4.1. Analysis of universality and applicability

To demonstrate the universality of this energy-saving renovation strategy, this study further analyzed the peak-shaving process results under other operating conditions (30 %, 40 %, 50 %, 75 %, 90 %, 100 %) and calculated the corresponding results using the Ebsilon steady-state model, as shown in Fig. 16. It can be observed that as the load increases, the boiler feedwater temperature changes almost linearly, and the increase becomes increasingly significant compared to before the renovation. Meanwhile, the coal consumption decreases uniformly with the rise in load, indicating that the energy-saving device has a positive impact on coal-fired units and further validating the effectiveness of this solution.

The ramp rate and minimum technical output of a power plant are core indicators of the flexibility of coal-fired plants. The ramp rate directly determines the speed at which a power plant responds to grid frequency control commands and affects the stability of the power system frequency. The minimum technical output reflects the deep peak shaving capability of a power plant and is a key constraint on the consumption of renewable energy. The two work together, a high ramp-up rate and low minimum technical output jointly enhance the dynamic regulation capability of a power plant in the low load zone and provide inertial support for the grid.

Through the above simulation analysis, the minimum technical output of the unit after modification is 34 % THA, which is higher than the minimum stable combustion threshold of 30 % THA. This proves that the stability of the modified unit is good. The specific formula for calculating the load ramping rate is as follows:

$$R_{ramp} = \frac{\Delta P}{P_{rated} \times \tau} \times 60 \tag{13}$$

$$\tau = \tau_0 \times e^{-0.012\times\left(T_{fw}-T_{fw0}\right)} \tag{14}$$

where R_{ramp} is the load ramp rate, % Pe/min; ΔP is the load step change; P_{rated} is the rated power; τ is the boiler inertia time constant; τ_0 is the inertia constant before modification; T_{fw0} is the feedwater temperature before modification; and T_{fw} is the feedwater temperature after modification. Combining the results under different working conditions in Fig. 16 and the above calculation formula, the load ramp rate before and after energy-saving retrofitting can be obtained as 3.95 % Pe/min and 4.43 % Pe/min, respectively, an increase of 12.16 %. This calculation proves that the retrofitting scheme has good practical grid adaptability.

3.4.2. Analysis of key economic indicators

In order to comprehensively assess the economic feasibility of the peak-shaving model and demonstrate the economic viability of the energy-savings retrofitting scheme, the calculation of key economic indicators can be further carried out. The total cost of energy-savings equipment and installation in this scheme was estimated to be 8.6 million by comparing it to the cost of the actual equipment [45]. The key economic indicators mainly include net present value (NPV), static payback period (SPBP) and levelized cost of electricity (LCOE)[46,47]. NPV provides a dynamic assessment of overall profitability, SPBP optimizes the capital turnover strategy, and LCOE ensures cost efficiency, which together provide a scientific basis for decision-makers to balance long-term profitability. The specific calculation formula is as follows [48,49]:

$$NPV = -C_{inv} + \sum_{t=1}^{T} \frac{R_{total,t} - C_{O\&M,t}}{(1+r)^t} + \frac{C_{sal}}{(1+r)^T} \tag{15}$$

$$SPBP = \frac{C_{inv}}{R_{total} - C_{O\&M}} \tag{16}$$

$$LCOE = \frac{C_{inv} + \sum_{t=1}^{T} C_{O\&M,t}\cdot(1+r)^{-t}}{\sum_{t=1}^{T} E_{peak,t}\cdot(1+r)^{-t}} \tag{17}$$

Where C_{inv} is the initial equipment investment cost, r is the discount rate, typically 8 %, $R_{total,t}$ and $C_{O\&M,t}$ are the peak-shaving revenue and annual maintenance cost in year t, respectively, and $E_{peak,t}$ is the amount of electricity peak-shaving in year t. C_{sal} is the salvage value, typically 5 % of the equipment cost.

The results of the key indicators can be obtained from the above formula, as shown in Table 9. It can be found that the NPV of the peak-shaving model coupled with energy-saving devices is 10.38 million CNY,

Table 9
Crucial economic indicators of economic analysis of peak-shaving model.

Indicators	Value
NPV (10,000CNY)	1037.92
SPBP (years)	0.45
$LCOE_{ES}$(CNY/kWh)	0.064

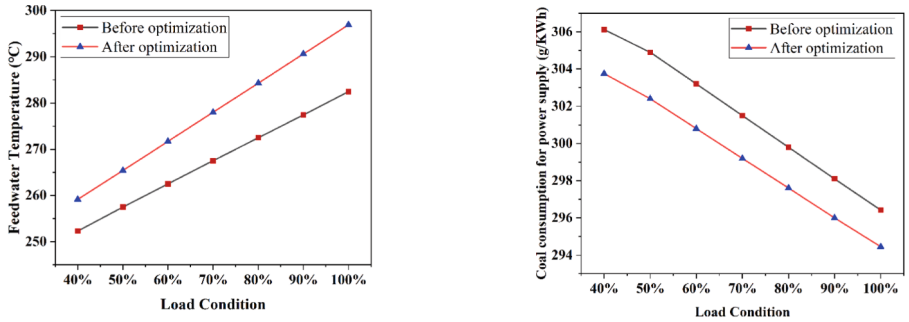

Fig. 16. Comparison of coal-fired units after energy-saving retrofits under different operating conditions: (a) Feedwater temperature and (b) Coal consumption for power supply.

indicating that the peak-shaving model has strong profitability, and the SPBP of the system is only 0.45 years, indicating that the peak-shaving system will return to the capital and begin to generate revenue in a short period. Currently, the LCOE is only 0.064 CNY/kWh, which significantly reduces the cost of power generation relative to the conventional CFPPs. Therefore, it can be proved that the peak-shaving model of the coupled with energy-saving devices has a better economy, which is conducive to guiding the subsequent practical application of the peak-shaving technology.

4. Conclusion

In this study, a typical 600 MW supercritical coal-fired unit is selected as the research object, and a model coupled with molten salt thermal storage for peak shaving is developed using process simulation. To further enhance the thermal efficiency of this integrated system, a synergistic energy-saving strategy that incorporates the HPH and FSC is introduced. The effects of No. 3 HPH feed steam parameters on boiler feedwater temperature and unit coal consumption are examined before and after implementing the energy-saving measures during both heat storage and release processes. Based on the energy-saving retrofitted scheme, a comprehensive peak-shaving and thermodynamic analysis of the integrated model is performed to establish unified design guidelines for flexible, economical, and high-performance peak shaving in thermal power plants.

The series heat storage/release mode effectively reduces system losses, lowering the coal consumption for power supply under 40 % THA conditions to 7805.15 kJ/kWh. The critical heat storage pressure is identified as 6 MPa, representing the economic turning point between high- and low-pressure steam extraction. The optimized steam extraction pressure for heat storage and the release pressure are determined to be 4 MPa and 8 MPa, respectively. With the implementation of energy-saving retrofitting, coal consumption decreases by 94.53 kJ/kWh during heat storage and by 24.62 kJ/kWh during heat release. Overall, the key economic indicators demonstrate that the peak-shaving model coupled with energy-saving devices delivers significantly improved economic performance.

The current integrated system faces three core challenges: the engine room layout needs to be reconfigured to accommodate thermal storage equipment, the low-temperature solidification characteristics of molten salt must be addressed to avoid restrictions on the minimum load of the unit, and the impact of high-temperature corrosion on system service life must be mitigated. Future research is expected to focus on molten salt-feedwater direct heat exchange technology to eliminate intermediate losses, as well as on the development of intelligent dynamic temperature control algorithms to optimize operating conditions, thereby unlocking the potential for deep peak shaving.

CRediT authorship contribution statement

Qilong Xu: Writing – original draft, Validation, Software, Investigation. **Shuai Wang:** Writing – review & editing, Methodology. **Kun Luo:** Writing – review & editing, Conceptualization. **Jianren Fan:** Supervision, Conceptualization.

Declaration of competing interest

The authors declare that they have no known competing financial interests or personal relationships that could have appeared to influence the work reported in this paper.

Acknowledgments

We are grateful for the support from the National Natural Science Foundation of China (588020-X42405; 52576174), Fundamental Research Funds for the Central Universities (226-2024-00138; 2022ZFJH004), and Key Research and Development Program of Zhejiang Province (2025C01047).

Appendix A. Supplementary material

Supplementary data to this article can be found online at https://doi.org/10.1016/j.applthermaleng.2025.128229.

Data availability

Data will be made available on request.

References

[1] X. Zhu, P. Gui, X. Zhang, Z. Han, Y. Li, Multi-objective optimization of a hybrid energy system integrated with solar-wind-PEMFC and energy storage, J. Storage Mater. 72 (2023) 108562, https://doi.org/10.1016/j.est.2023.108562.
[2] J. Wang, Y. Wen, K. Wu, S. Ding, Y. Liu, H. Tian, et al., Optimization study of wind, solar, hydro and hydrogen storage based on improved multi-objective particle swarm optimization, J. Storage Mater. 93 (2024) 112298, https://doi.org/10.1016/j.est.2024.112298.
[3] A. Zahoor, F. Mehr, G. Mao, Y. Yu, A. Sápi, The carbon neutrality feasibility of worldwide and in China's transportation sector by E-car and renewable energy sources before 2060, J. Storage Mater. 61 (2023) 106696, https://doi.org/10.1016/j.est.2023.106696.
[4] M. Xiang, Y. Zhang, C. Li, C. Qi, Peak-shaving cost of power system in the key scenarios of renewable energy development in China: Ningxia case study, J. Storage Mater. 91 (2024) 112133, https://doi.org/10.1016/j.est.2024.112133.
[5] H.R. Thakare, P. Daspute, Enhancing energy conservation in power generation in a coal fired thermal power plant through comprehensive energy audit, Energy 301 (2024) 131661, https://doi.org/10.1016/j.energy.2024.131661.
[6] Q. Zheng, H. Chen, H. Wu, H. Zheng, P. Pan, J. Bian, et al., Performance analysis of a medical waste gasification-based power generation system integrated with a coal-fired power unit considering dispatching optimization, Energy 310 (2024) 133200, https://doi.org/10.1016/j.energy.2024.133200.
[7] Z. Mu, Y. Lv, K. Jiang, Q. Zhang, Q. Wang, F. Fang, et al., A dynamic nonlinear model for controller design of flue gas-molten salt heat exchanger in flexibility retrofit coal-fired unit, J. Storage Mater. 101 (2024) 113897, https://doi.org/10.1016/j.est.2024.113897.
[8] C. Wang, Z. Liu, M. Fan, Y. Zhao, M. Liu, J. Yan, Enhancing the flexibility and efficiency of a double-reheat coal-fired power unit by optimizing the steam temperature control: from simulation to application, Appl. Therm. Eng. 217 (2022) 119240, https://doi.org/10.1016/j.applthermaleng.2022.119240.
[9] H. Wang, J. Han, R. Zhang, M. Sun, Z. Sun, P. Hua, et al., Heat-power peak shaving and wind power accommodation of combined heat and power plant with thermal energy storage and electric heat pump, Energ. Conver. Manage. 297 (2023) 117732.
[10] C. Wang, J. Song, Performance assessment of the novel coal-fired combined heat and power plant integrating with flexibility renovations, Energy 263 (2023) 125886, https://doi.org/10.1016/j.energy.2022.125886.
[11] Q. Xu, X. Li, J. Yu, S. Wang, K. Luo, J. Fan, Optimization of parameters and thermodynamics of gasification process for enhanced CO_2 capture in an IGCC system, Energy 304 (2024) 131853, https://doi.org/10.1016/j.energy.2024.131853.
[12] Q. Xu, S. Wang, K. Luo, Y. Mu, L. Pan, J. Fan, Process modelling and optimization of a 250 MW IGCC system: ASU optimization and thermodynamic analysis, Energy 282 (2023) 128864, https://doi.org/10.1016/j.energy.2023.128864.
[13] J. Xu, Q. Zhang, N. Ye, Z. Zhang, X. Wu, H. Fan, A review on flexible peak shaving development of coal-fired boilers in China under the carbon peak and carbon neutrality goals, Therm. Sci. Eng. Prog. 55 (2024) 103004, https://doi.org/10.1016/j.tsep.2024.103004.
[14] Y. Cui, K. Jiang, H. Wei, X. Du, A steam combination extraction thermal energy storage scheme in boiler side for coal-fired power plant flexibility retrofit, J. Storage Mater. 98 (2024) 113038, https://doi.org/10.1016/j.est.2024.113038.
[15] D. Wang, D. Liu, C. Wang, Y. Zhou, X. Li, M. Yang, Flexibility improvement method of coal-fired thermal power plant based on the multi-scale utilization of steam turbine energy storage, Energy 239 (2022) 122301, https://doi.org/10.1016/j.energy.2021.122301.
[16] R. Cao, Y. Lu, D. Yu, Y. Guo, W. Bao, Z. Zhang, et al., A novel approach to improving load flexibility of coal-fired power plant by integrating high temperature thermal energy storage through additional thermodynamic cycle, Appl. Therm. Eng. 173 (2020) 115225.
[17] M. Fochesato, C. Peter, L. Morandi, J. Lygeros, Peak shaving with hydrogen energy storage: from stochastic control to experiments on a 4 MWh facility, Appl. Energy 376 (2024) 123965, https://doi.org/10.1016/j.apenergy.2024.123965.
[18] X. Chen, E. Oko, X. Wu, Integration and capacity optimization of molten-salt heat storage in coal-fired power plant with carbon capture system, J. Storage Mater. 99 (2024) 113363, https://doi.org/10.1016/j.est.2024.113363.
[19] K. Jiang, G. Zhang, H. Liu, Z. Mu, Q. Wang, T. Qin, et al., Design and dynamic simulation of flue gas-molten salt heat exchanger in flexible operation coal-fired power plant, J. Storage Mater. 93 (2024) 112227, https://doi.org/10.1016/j.est.2024.112227.

[20] L. Zhu, Z. Zhong, C. Wang, J. Song, J. Guo, W. Zheng, Thermo-economic comparison of integrating compressed air energy storage and molten salt thermal energy storage in a combined heat and power plant, Appl. Therm. Eng. 260 (2025) 124931, https://doi.org/10.1016/j.applthermaleng.2024.124931.
[21] T. Ma, Z. Li, K. Lv, D. Chang, W. Hu, Y. Zou, Design and performance analysis of deep peak shaving scheme for thermal power units based on high-temperature molten salt heat storage system, Energy 288 (2024) 129557.
[22] Q. Zhang, K. Jiang, Z. Ge, L. Yang, X. Du, Control strategy of molten salt solar power tower plant function as peak load regulation in grid, Appl. Energy 294 (2021) 116967, https://doi.org/10.1016/j.apenergy.2021.116967.
[23] G. Humbert, C. Roosendaal, J.K. Swanepoel, H.M. Navarro, W.G. Le Roux, A. Sciacovelli, Development of a latent heat thermal energy storage unit for the exhaust of a recuperated solar-dish Brayton cycle, Appl. Therm. Eng. 216 (2022) 118994, https://doi.org/10.1016/j.applthermaleng.2022.118994.
[24] X. Meng, S. Zhang, H. Liu, S. Zhou, A method of energy storage capacity planning to achieve the target consumption of renewable energy, J. Storage Mater. 97 (2024) 112993, https://doi.org/10.1016/j.est.2024.112993.
[25] S. Zhang, M. Liu, Y. Zhao, J. Liu, J. Yan, Energy and exergy analyses of a parabolic trough concentrated solar power plant using molten salt during the start-up process, Energy 254 (2022) 124480, https://doi.org/10.1016/j.energy.2022.124480.
[26] K. Hood, M. Walsh, A. Zolan, G. Jackson, A. Newman, Characterizing and improving the performance of molten-salt-steam heat exchangers in concentrating solar power plants, Energ. Conver. Manage. 315 (2024) 118721, https://doi.org/10.1016/j.enconman.2024.118721.
[27] J. Xu, W. Liu, Z. Wang, S. Ma, G. Zhao, Y. Gu, Comparative investigation on the thermodynamic performance of coal-fired power plant integrating with the molten salt thermal storage system, J. Storage Mater. 89 (2024) 111738, https://doi.org/10.1016/j.est.2024.111738.
[28] Q. Zhang, J. Dong, H. Chen, F. Feng, G. Xu, X. Wang, et al., Dynamic characteristics and economic analysis of a coal-fired power plant integrated with molten salt thermal energy storage for improving peaking capacity, Energy 290 (2024) 130132.
[29] B. Wang, H. Ma, S. Ren, F. Si, Effects of integration mode of the molten salt heat storage system and its hot storage temperature on the flexibility of a subcritical coal-fired power plant, J. Storage Mater. 58 (2023) 106410, https://doi.org/10.1016/j.est.2022.106410.
[30] R. Bartnik, A. Hnydiuk-Stefan, Evaluation of energy and economic efficiency in upgrading coal-fired power plants: Integrating HTGR reactors and turboexpanders for supercritical steam parameters, Energy 318 (2025) 134763, https://doi.org/10.1016/j.energy.2025.134763.
[31] J. Li, X. Li, P. Yan, G. Zhou, J. Liu, D. Yu, Thermodynamics, flexibility and techno-economics assessment of a novel integration of coal-fired combined heating and power generation unit and compressed air energy storage, Appl. Energy 339 (2023) 120924, https://doi.org/10.1016/j.apenergy.2023.120924.
[32] Z. Liu, W. Zhong, X. Liu, Y. Shao, Techno-economic and environmental evaluation of a supercritical CO_2 coal-fired circulating fluidized bed boiler power generation, Energy 285 (2023) 129470, https://doi.org/10.1016/j.energy.2023.129470.
[33] D. Lai, C. Luo, Z. Wang, Z. Shi, T. Luo, L. Zhang, et al., Process simulation and techno-economic analysis of CO_2 capture by coupling calcium looping with concentrated solar power in coal-fired power plant, Sep. Purif. Technol. 358 (2025) 130228, https://doi.org/10.1016/j.seppur.2024.130228.
[34] Y. Fu, Y. Huang, H. Xin, M. Liu, L. Wang, J. Yan, The pressure sliding operation strategy of the carbon capture system integrated within a coal-fired power plant: influence factors and energy saving potentials, Energy 307 (2024) 132737, https://doi.org/10.1016/j.energy.2024.132737.
[35] Y. Li, Y. Wang, L. Cao, P. Hu, W. Han, Modeling for the performance evaluation of 600 MW supercritical unit operating No.0 high pressure heater, Energy 149 (2018) 639–661, https://doi.org/10.1016/j.energy.2018.01.103.
[36] Y. Zhao, C. Wang, M. Liu, D. Chong, J. Yan, Improving operational flexibility by regulating extraction steam of high-pressure heaters on a 660 MW supercritical coal-fired power plant: a dynamic simulation, Appl. Energy 212 (2018) 1295–1309, https://doi.org/10.1016/j.apenergy.2018.01.017.
[37] C. Wu, Q. Wang, X. Wang, S. Sun, D. Cui, S. Pan, et al., Thermodynamic calculations and experimental studies of ternary molten salts for high-temperature thermal energy storage, J. Storage Mater. 73 (2023) 109220, https://doi.org/10.1016/j.est.2023.109220.
[38] H.A. Aljaerani, M. Samykano, A.K. Pandey, K. Kadirgama, M. George, R. Saidur, Thermophysical properties enhancement and characterization of CuO nanoparticles enhanced HITEC molten salt for concentrated solar power applications, Int. Commun. Heat Mass Transfer 132 (2022) 105898, https://doi.org/10.1016/j.icheatmasstransfer.2022.105898.
[39] P.D. Tagle-Salazar, L.F. Cabeza, C. Prieto, Transient performance modelling of solar tower power plants with molten salt thermal energy storage systems, J. Storage Mater. 97 (2024) 112793, https://doi.org/10.1016/j.est.2024.112793.
[40] M. Pater, B. Kaaks, B. Lauritzen, D. Lathouwers, A numerical benchmark for modelling phase change in molten salt reactors, Ann. Nucl. Energy 194 (2023) 110093, https://doi.org/10.1016/j.anucene.2023.110093.
[41] S. Lv, Y. Lu, Y. Ma, Y. Cui, Z. Wang, Y. Wu, et al., Design and performance analysis of peak shaving mode for coal-fired power unit based on the molten salt thermal energy storage system, J. Storage Mater. 104 (2024) 114491, https://doi.org/10.1016/j.est.2024.114491.
[42] Z. Liu, C. Wang, J. Fan, M. Liu, Y. Xing, J. Yan, Enhancing the flexibility and stability of coal-fired power plants by optimizing control schemes of throttling high-pressure extraction steam, Energy (2024), https://doi.org/10.1016/j.energy.2023.129756.
[43] H. Wei, Y. Lu, Y. Yang, C. Zhang, C. He, Y. Wu, et al., Research on influence of steam extraction parameters and operation load on operational flexibility of coal-fired power plant, Appl. Therm. Eng. 195 (2021) 117226, https://doi.org/10.1016/j.applthermaleng.2021.117226.
[44] Q. Xu, S. Wang, K. Luo, Y. Mu, L. Pan, J. Fan, Process modelling and optimization of a 250 MW IGCC system: model setup, validation, and preliminary predictions, Energy 272 (2023) 127040, https://doi.org/10.1016/j.energy.2023.127040.
[45] J.J. Lee, S.Y. Kang, T.S. Kim, S.S. Byun, Thermo-economic analysis on the impact of improving inter-stage packing seals in a 500 MW class supercritical steam turbine power plant, Applied Thermal Engineering 121 (2017) 974–983.
[46] Y. Chen, Y. Wu, X. Liu, J. Ma, D. Liu, X. Chen, D. Liu, Energy, exergy and economic (3E) analysis of a novel integration process based on coal-fired power plant with CO_2 capture & storage, CO_2 refrigeration, and waste heat recovery, Energy 299 (2024), https://doi.org/10.1016/j.energy.2024.131443.
[47] W. Liao, X. Zhang, H. Ke, S. Zhang, J. Shao, H. Yang, et al., The techno-economic-environmental analysis of a pilot-scale positive pressure biomass gasification coupled with coal-fired power generation system, J. Clean. Prod. 402 (2023) 136793, https://doi.org/10.1016/j.jclepro.2023.136793.
[48] Y. Wang, H. Chen, T. Li, P. Pan, R. Zhai, G. Xu, et al., Thermo-economic analysis of a waste-to-energy assisted carbon capture system for a coal-fired power plant, Appl. Therm. Eng. 229 (2023) 120594, https://doi.org/10.1016/j.applthermaleng.2023.120594.
[49] M. Cossutta, S. Pholboon, J. McKechnie, M. Sumner, Techno-economic and environmental analysis of community energy management for peak shaving, Energ. Conver. Manage. 251 (2022) 114900, https://doi.org/10.1016/j.enconman.2021.114900.